Available online at www.sciencedirect.com
SCIENCE DIRECT®
Biochemical Pharmacology 67 (2004) 1035–1045
Biochemical Pharmacology
www.elsevier.com/locate/biochempharm

Subcellular localization of the camptothecin analogues, topotecan and gimatecan

Anna Cleta Croce[a], Giovanni Bottiroli[a], Rosanna Supino[b], Enrica Favini[b], Valentina Zuco[b], Franco Zunino[b,*]

[a]*IGM-CNR, Sezione di Istochimica e Citometria, Dipartimento di Biologia Animale, Università di Pavia, 27100 Pavia, Italy*
[b]*Istituto Nazionale Tumori, 20133 Milan, Italy*

Received 6 June 2003; accepted 23 October 2003

Abstract

Lipophilicity of camptothecins derivatives has been reported to improve the stability of the lactone ring and to favor rapid uptake and intracellular accumulation. Recently, a novel series of lipophilic camptothecins substituted at position 7 was developed, and gimatecan (ST1481) was selected for clinical development on the basis of some favorable features, including potent cytotoxicity and the unique feature of the lack of recognition by breast cancer resistance-associated protein (BCRP). In this work the intrinsic fluorescence properties of this compound were exploited to investigate its intracellular disposition in comparison with the water-soluble camptothecin, topotecan (TPT), in HT-29 colon carcinoma cells and in a subline, HT-29/Mit, selected for resistance to mitoxantrone and overexpressing BCRP. The study was performed at single-cell level by means of microspectrofluorometry and fluorescence image analysis. The results indicated a quite different subcellular localization of TPT ST1481, since TPT localized mainly in mitochondria, whereas gimatecan exhibited a lysosomal localization. An increased persistence of DNA damage in gimatecan-treated cells was consistent with the interpretation that lysosomes represent a store of active drug. In contrast to gimatecan, which showed a similar localization in HT-29 cells and in the mitoxantrone-resistant subline, the cellular pharmacokinetic of TPT was markedly influenced by overexpression of BCRP protein in the resistant subline. In conclusion, the present results indicating a quite different behavior of the two camptothecins suggest that, apart from intracellular accumulation, subcellular distribution plays a role in their cytotoxic potency and contributes to their pharmacological features.

Keywords: Camptothecins; Subcellular localization; BCRP; Resistance; Colon carcinoma cells

1. Introduction

The interest in camptothecins is related to their efficacy in a wide range of solid tumors and to the recognition that topoisomerase I, a critical enzyme in several DNA functions, is an useful target for the design of effective antitumor agents [1,2]. Much effort has been devoted to improve water solubility of camptothecins and two water-soluble analogs (TPT and irinotecan) are now in clinical practice. However, lipophilicity has been reported to improve the stability of the lactone ring and to favor rapid uptake and intracellular accumulation. Recently, a novel series of lipophilic camptothecins substituted at position 7 was developed [3]. Among the analogues of this series, ST1481 was selected for clinical development on the basis of some favorable features, including potent cytotoxicity, stability of the topoisomerase I-mediated cleavable complex, oral bioavailability, efficacy and tolerability in a large panel of tumor models [4]. An unique feature of the novel analogue is the lack of recognition by breast cancer resistance-associated protein (BCRP) [5], a transport system implicated not only in modulation of cellular sensitivity but also in intestinal absorption of exogenous compounds [6]. On the basis of these observations, the present study was designed to compare the intracellular dispositions of a water-soluble camptothecin, TPT, and of the lipophilic analogue, ST1481, in HT-29

* Corresponding author. Tel.: +39-02-23902267; fax: +39-02-23902692.
E-mail address: franco.zunino@istitutotumori.mi.it (F. Zunino).
Abbreviations: a.u., arbitrary units; F.I., fluorescence intensity; TPT, topotecan; BCRP, breast cancer resistance-associate protein.

0006-2952/$ – see front matter © 2003 Elsevier Inc. All rights reserved.
doi:10.1016/j.bcp.2003.10.034

colon carcinoma cells and in a subline selected for resistance to mitoxantrone and overexpressing BCRP. The cellular pharmacology of the two camptothecin analogs was substantially different, because the lipophilic derivative exhibited an increased cellular uptake without defects in intracellular accumulation by BCRP-overexpressing cells. The results of this cellular pharmacology study, indicating a quite different behavior of the two agents, suggest that not only intracellular accumulation but also subcellular distribution plays a role in the cytotoxic potency.

2. Materials and methods

2.1. Chemicals, drugs and cells

The ST1481 (7-*t*-butoxyminomethylcamptothecin) was provided by Sigma-Tau and was dissolved in DMSO 10%. TPT (Smith-Kline Beecham Pharmaceuticals) was dissolved in water before the use. The final concentration of DMSO in culture medium did not exceed the 0.2%. Dioxane is from Riedel De Haen AG Seelze, and bovine serum albumin from Sigma Chem. Co.

HT-29 and HT-29/Mit were maintained as monolayers in RPMI 1640 medium supplemented with 10% fetal calf serum. HT-29/Mit was a mitoxantrone-resistant subline of HT-29 obtained by exposure to increasing concentrations of mitoxantrone [5].

2.2. Spectral analysis in solution

TPT and ST1481 were diluted in phosphate buffer (0.1 M, pH 5.7, 6.4 or 7.4) to the concentration of 5 and 2 μg/mL for absorption and fluorescence spectroscopy analysis, respectively. Absorption spectra were recorded in the 300–480 nm range by means of a Spectronic Genesys Spectrophotometer (Spectronic Instruments Inc.). Fluorescence excitation and emission spectra were recorded in the 300–430 nm and 400–650 nm ranges, respectively, by means of a spectrofluorimeter (model SP-2; Applied Photophysics), equipped with a single photon counting system (EG&G-Ortec).

2.3. Microspectrofluorometric analysis

Microspectrofluorometric analysis was performed under epi-illumination condition by means of a Leitz microspectrograph, equipped with an Optical Multichannel Analyzer (OMA III, EG&G, Princeton Applied Research) employing a Jarrell-Ash Monospec 27 spectrograph (Allied Analytical System; mod. 82-499, H150 g/mm grating) and a 512-element intensified diode array detector (mod. 1420/512). Fluorescence excitation light was provided by a 100 W Hg lamp (Osram), combined with KG1 and BG38 antithermal filters. Excitation wavelength was selected by means of a 366 nm interference filter ($T\% = 40$) and a 390 nm dichroic mirror ($T_{366} < 2\%$). The fluorescence emission was filtered through a 386 nm barrier filter, and spectra were recorded in the 420–700 nm range. The emission spectra of the drug were obtained subtracting the spectra recorded on treated cells by the autofluorescence contribution as measured on untreated cells.

2.4. Image analysis

Fluorescence images were acquired by means of an Argus VIM 100 processor digital system (Hamamatsu Photonics Deutschland GmbH, Herrsching am Ammersee), using an high sensitive ISIT camera (Hamamatsu C2400-09) coupled to a Leitz fluorescence microscope. The images were digitally stored on a magnetic mass memory support and processed by means of the Hamamatzu Argus 100 control program.

For drug localization study, images under excitation at 366 nm (366 nm interference filter; $T\% = 40$) were acquired in the 440–520 nm spectral region (Kodak Wratten filter n. 45) for TPT, ST1481, Rhodamine 123 and Lucifer Yellow, and beyond 570 nm (RG 570 barrier filter) for LysoTracker Red.

2.5. Drug uptake and release studies

For drug uptake and release studies the cells were seeded on slides in six multiwell plates. Cells were incubated with TPT or ST1481, 10 μg/mL, diluted in the medium directly from stock solutions (2 mg/mL). At prefixed times the slides were removed from the incubation medium, washed with PBS, and submitted immediately to microspectrofluorometric or image analysis, performed under vital conditions. Microspectrofluorometric data were corrected for the autofluorescence contribution as evaluated on untreated cells. Two independent experiments were performed in duplicate. At least 30 cells were measured for each incubation time.

The intracellular drug amount was determined in terms of fluorescence intensity. For ST1481 the fluorescence intensity was measured in the 480 ± 20 nm spectral range. In the case of TPT, since the spectral profile changed during incubation time indicating the presence of two spectral components, a curve-fitting procedure was applied in order to evaluate the weight of each single component contributing to the overall emission.

Spectra were analyzed by means of an iterative non-linear curve-fitting procedure (PeakFit; SPSS Science) based on the Marquardt–Levenberg algorithm [7], through the finding of the true absolute minimum value of the sum of squared deviations (χ^2). Fitting analysis was performed using a linear combination of half-Gaussian Modified Gaussian (GMG) spectral functions. GMG spectral function representing the emission band at 525 nm was defined by parameters derived from the real spectra of the pure TPT

in buffer solution (pH 7.4) through subsequent adjustments to match the best fit for the line shape of the spectrum (peak center wavelength: 525 nm; full width at half intensity maximum: 105 nm). The emission band centered at about 470 nm was represented by means of an additional GMG spectral function, calculated by subtracting the 525 nm GMG from the whole spectrum corresponding to the mean of the spectra taken from resistant cells at 180 nm of uptake. A GMG spectral function with a 468 nm peak center wavelength and a 89 nm full width at half intensity maximum was obtained that was quite constant for all the spectra recorded from the cells under the different experimental conditions.

The parameter values obtained were then used to define the relative contribution of each single spectral component to the whole fluorescence emission. After a first subjective matching of the contribution of the individual GMG bands, the fit of the spectral components was adjusted and verified by the iterative process, until a satisfying goodness of fit was obtained, according to both correlation r^2 and residual analysis.

2.6. Cell organelle staining

To identify the sites of drug localization, specific organelle stainings were performed on living cells. In particular, for mitochondria identification, cells were incubated with Rhodamine 123, 2 μg/mL, 5 min (Sigma Chemical Co); for endosomal and endoplastic compartments identification, cells were incubated with Lucifer Yellow, 10 μg/mL, 15 min (Sigma Chemical Co) and dried before image analysis; for lysosomes identification, cells were exposed to LysoTracker Red DND-99 (Molecular Probes), 1 μM, for 40 min before the cells collection for image analysis.

The organelles involved in the drugs localization were identified through a comparative analysis of the fluorescence patterns of cells treated with TPT or ST1481, or stained with the above described specific organelle markers. The low quantum efficiency of TPT and the partial overlapping of the fluorescence emission of the drugs with that of the dyes, in fact, did not allow a reliable colocalization study. Only in the case of ST1481 a contemporary cell staining with the drug and LysoTracker Red was performed, thanks to the good quantum efficiency of ST1481.

2.7. BCRP localization

Cells seeded on glass as above described, were fixed in acetone 100% for 15 min. After washing in phosphate buffered solution containing 1% bovine serum albumin, cells were incubated with the anti-BCRP antibody (Alexis Biochemicals) diluted 1:50 for 45 min, and labeled with an anti-mouse FITC antibody for 30 min. Samples were rinsed with PBS, mounted in Mowiol, and submitted to BCRP localization study. The confocal microscopy analysis was performed by means of a Leica TCS SP2 Laser Scanning Confocal System (Leica Company), fitted on a Leica DM IRBE inverted microscope (63× oil objective, N.A. 3.2). Excitation was provided by the 488 nm Argon ion laser line, and fluorescence emission was collected in the 500–550 nm range. Every image was collected with a format of 1024 × 1024 pixels. Stacks of images of serial optical sections along the *z*-axis were collected with a step size of 0.45 μm. Images were stored on a magnetic mass memory and processed by means of the Leica Confocal Software.

2.8. Intracellular drug distribution

Quantitative analysis of TPT and ST1481 intracellular distribution was performed on images acquired through a 430 nm barrier filter under excitation at 366 nm. The drug subcellular localization was evaluated in selected regions corresponding to granules, cytoplasm and nucleus. Granules were discriminated as defined structures showing a brighter fluorescence emission in comparison with the surrounding cellular areas (cytoplasm). Measurements were performed integrating pixel-by-pixel the fluorescence signal of fixed areas, selected according to the dimension of the smallest structure, i.e. granules. For each region considered, data are reported as fluorescence intensity mean values for pixel unit. At least 20 cells were considered for each incubation time, for two separate experiments performed in duplicate.

2.9. Alkaline elution

DNA single-strand breaks were determined by the alkaline elution method [8]. Cellular DNA was labeled with 0.08 μCi/mL [2-^{14}C]thymidine (Amersham) for 30 hr. After further 18 hr in the absence of labeled thymidine, cells were exposed to the drugs (IC_{80}) for 1 hr and then processed immediately or incubated in drug-free medium up to 3 hr. Cells irradiated with 400 rad were used as positive control.

3. Results

3.1. Spectral analysis in solution

The absorption, excitation and emission properties of the two drugs were analyzed under different pH and polarity conditions. Absorption/excitation spectral shape of TPT was pH-dependent (Fig. 1A and C), whereas the emission profile was pH-independent (Fig. 1C). In particular, at pH 5.7 and 6.4 the main absorption band was found at about 385 nm and minor bands were observed at 330 and 370 nm; at pH 7.4 three bands with comparable amplitudes were found at 340, 390 and 420 nm (Fig. 1A). As to excitation, at pH 5.7 and 6.4 the band was found at about 375 nm and minor bands were observed at 320 and

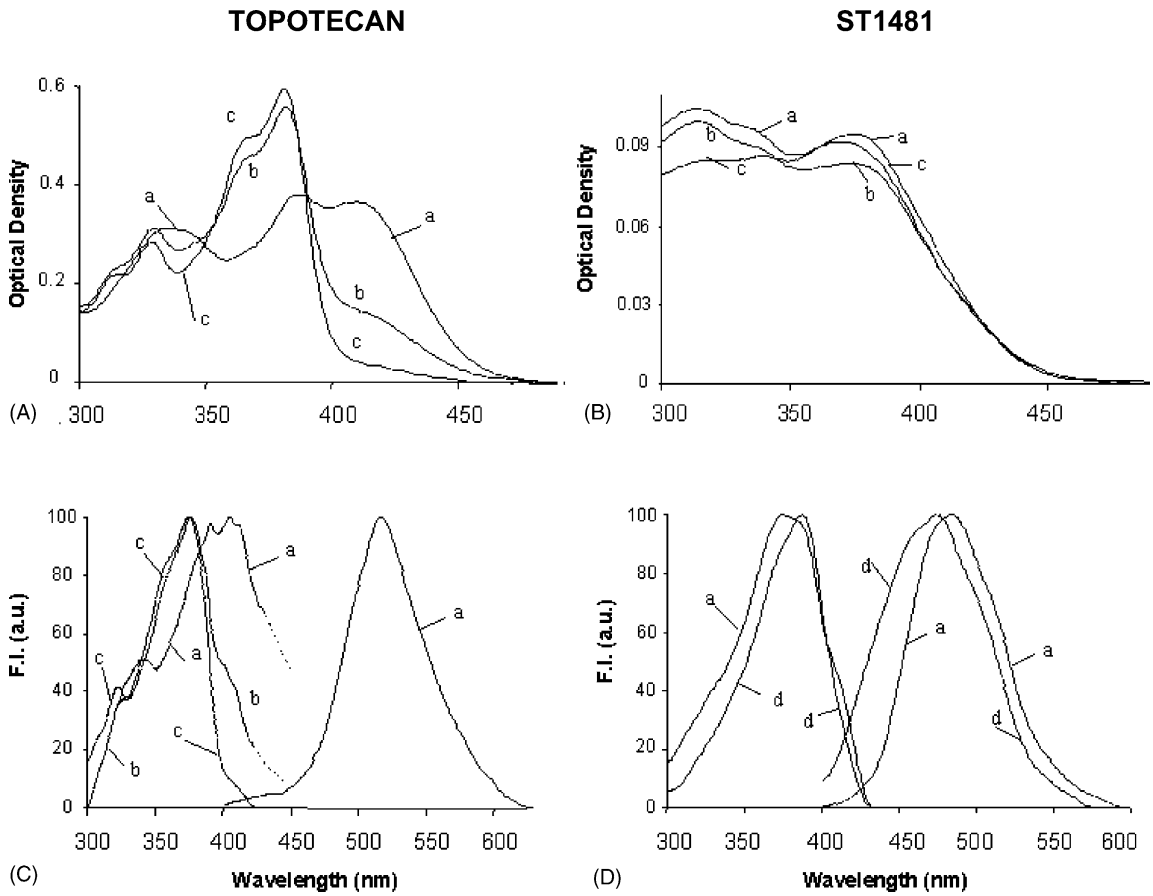

Fig. 1. Absorption and fluorescence spectra of topotecan (A, C) and ST1481 (B, D). Absorption and fluorescence excitation (left) and emission (right) spectra were recorded in phosphate buffer solution, pH 7.4 (a), 6.4 (b), and 5.7 (c) or after addition of 10 mg/mL albumin in pH 7.4 phosphate buffer solution (d). Fluorescence spectra are normalized to the peak maximum values.

355 nm; at pH 7.4 three main bands were found in the 390–420 nm region, with a minor band at 340 nm (Fig. 1C). The emission spectrum in solution at pH 7.4 is shown in Fig. 1C and the spectra at pH 6.4 or 5.7 were quite similar (not shown). The fluorescence quantum efficiency was found to be dependent on the pH value: under excitation at 370 nm the fluorescence intensity of the solution at pH 7.4 was 1.5 times larger than that at pH 5.7, being the absorption values of the two solutions the same. Addition of albumin (10 mg/mL) to drug solution at pH 7.4 resulted in a blue-shift (about 2 nm) of the TPT emission spectrum along with the appearance of a small shoulder at wavelengths shorter than 470 nm (data not shown). The small spectral changes above described were accompanied by an increase in the fluorescence intensity by about 40%. On the contrary, addition of DNA (0.1 mg/mL) in the buffer solution (pH 7.4) did not induce appreciable alterations either of the shape of the spectrum or of the emission intensity of TPT, in agreement with data already reported [9]. In a low polarity medium such as dioxane excitation spectrum exhibited a profile quite similar to that obtained in buffer solution at pH 5.7 and 6.4, but is red-shifted by about 12 nm. The emission spectrum was blue-shifted by about 25 nm (data not shown) and the emission intensity increased by about 10 times with respect to buffer solutions.

Spectral analysis of ST1481 indicated that: (i) absorption/excitation spectra were pH-dependent, although to a lesser extent than that observed for TPT, whereas the emission are pH independent (Fig. 1B and D). In particular, absorption spectra show two main bands centered at about 315 and 370 nm (Fig. 1B), whereas fluorescence excitation spectrum exhibits a band centered at about 370 nm, with a shoulder at about 390 nm (Fig. 1D). The emission spectra recorded at pH 7.4, 6.4 and 5.7 are quite similar and exhibited a maximum at about 485 nm. The emission spectrum at pH 7.4 is shown in Fig. 1D; (ii) addition of albumin (10 mg/mL), favored the excitation band at 390 nm, and induced a blue-shift of the emission spectrum-peak at 460 nm with the appearance of a shoulder at wavelengths shorter than 455 nm. A marked increase in the quantum efficiency was also found. No spectral changes were observed upon addition of DNA; (iii) low polarity medium dioxane favored the excitation band at 390 nm, and induced a much more marked blue-shift of the emission band, that is centered at about 463 nm. The quantum efficiency increased more than 10 times with respect to aqueous solution.

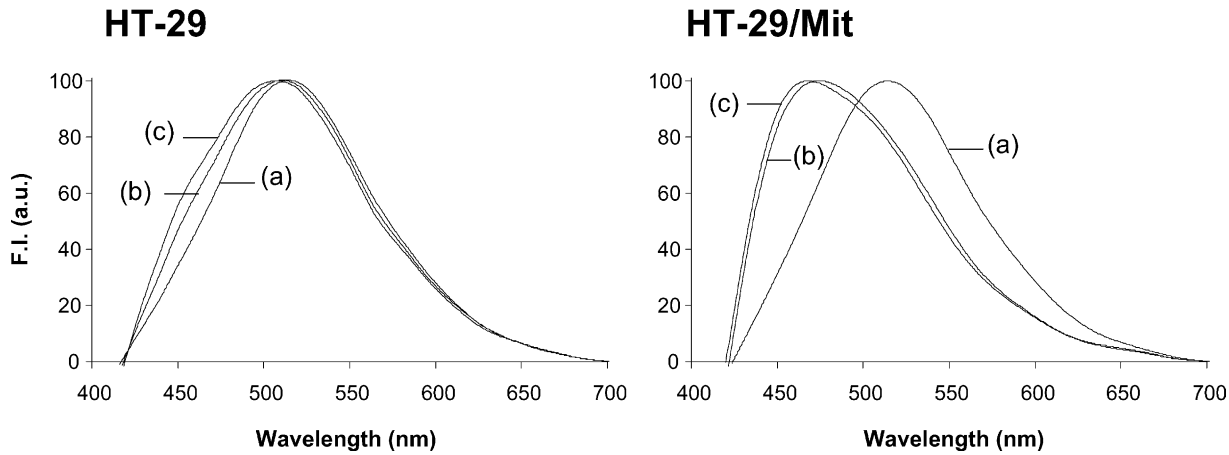

Fig. 2. Fluorescence emission spectra recorded from HT-29 and HT-29/Mit cells after TPT treatment. Incubation times: 30 min (a); 60 min (b); 180 min (c). Spectra are subtracted for the natural fluorescence signal, and normalized to the peak maximum value.

These results indicate that the fluorescence properties of both drugs are sensitive to the medium polarity. In particular, reduction of medium polarity results in a blue-shift of the emission spectrum and in an increase in the fluorescence quantum efficiency.

3.2. Microspectrofluorometry in cells

Microspectrofluorometric analysis of cells incubated with TPT (10 μg/mL) for different times showed changes in the spectral emission shape for both cell lines. The subtraction of the natural fluorescence contribution—as measured on untreated cells—from the spectrum of treated cells showed that the shape of the emission attributable to TPT varied depending on the incubation time (Fig. 2). A curve-fitting procedure, based on the parameters of the fluorescence spectra recorded in solution, showed that this emission consists exclusively of two main bands centered at about 470 and 525 nm (Fig. 3). These bands are consistent with a localization of TPT in hydrophobic or hydrophilic environment, respectively. The curve-fitting procedure allowed to define the relative contribution of each spectral component to the overall emission.

The fluorescence time course of each of the two bands was determined in single cells during drug uptake (Fig. 4). For both cell lines the time course of the TPT fraction localized in hydrophilic sites (525 nm emission band) showed a maximum at 30 min of drug exposure, followed by a decrease at the longer times. In HT-29 cells the emission signal was reduced to about 50% at 60 min, and remained almost constant up to 180 min. HT-29/Mit cells exhibited emission intensity values much lower than HT-29 cells at 30 min uptake. The difference was less evident at longer incubation times.

As to the 470 nm emission band (TPT fraction localized in hydrophobic sites), HT-29/Mit cells still exhibited emission intensity values lower than HT-29 cells at 30 min, although the difference was lesser than that found for the 525 nm band. At longer times the values in HT-29/Mit cells were even much higher than those in HT-29 cells. This finding can be explained taking into account the spectral changes occurring in the two cell lines during time, being the hydrophobic localization favored in HT-29/Mit cells.

Studies on drug retention performed after incubation of drug-treated cells in drug-free medium showed that, for

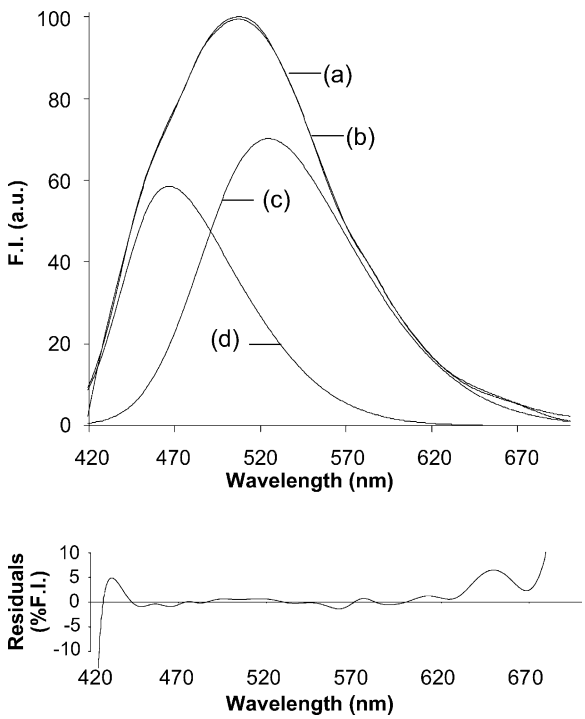

Fig. 3. Curve-fitting analysis of a typical spectrum recorded from HT-29 cell after 180 min TPT incubation. Upper panel: curves measured (a) and generated from the fitting (b), and bands representative for the best fit of pure TPT (c) in buffer solution (pH 7.4) and for the 470 nm band GMG spectral function (d). Lower panel: residuals, showing the differences between the fitted and the measured curves, are displayed as a percentage of the F.I. data values. Fitting r^2 coefficient of determination = 0.998.

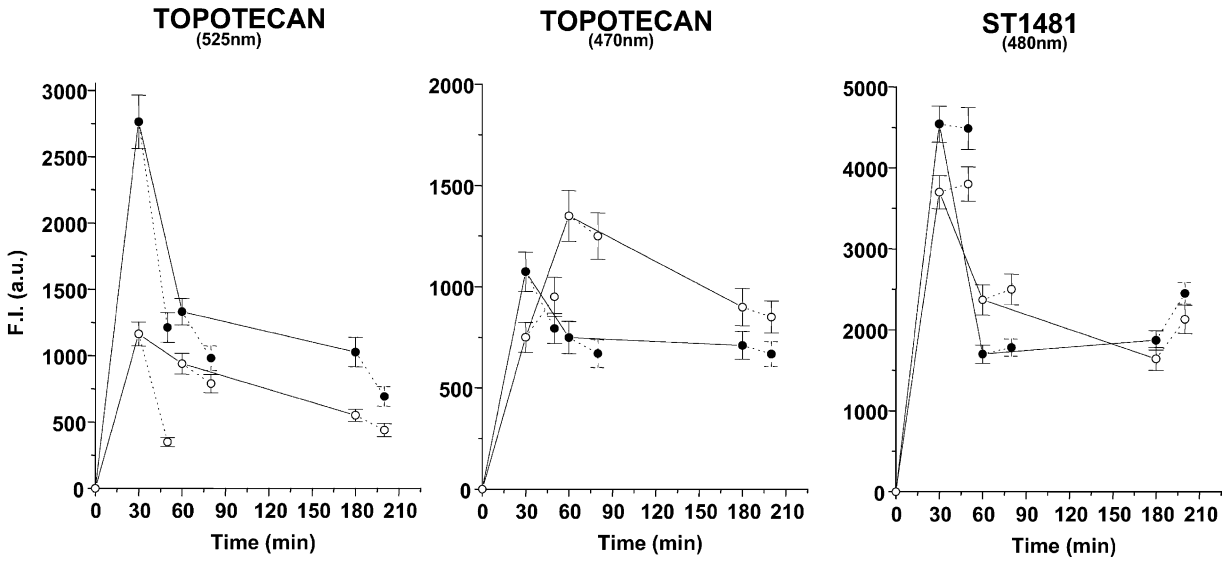

Fig. 4. Time course of fluorescence intensity values in HT-29 (●) and HT-29/Mit (○) single cells, during ST1481 or TPT exposure (10 μg/mL) (—), and subsequent incubation in drug-free medium (- - - -). Values were determined, through microspectrofluorimetric analysis, at 480 ± 20 nm for ST1481 and at 525 and 470 nm for spectral components of TPT. Mean values ± SE.

both cell lines, the signal of the 525 nm emission band (TPT fraction localized in hydrophilic sites) undergoes a rapid decrease after 30 min drug exposure. The decrease was less marked for cells after 60 and 180 min drug exposures. The signal relative to the TPT fraction localized in hydrophobic sites (470 nm) exhibited a similar trend for all drug-exposure times only in the case HT-29 line. In HT-29/Mit line an increase in fluorescence signal occurred in cells incubated in drug-free medium after the 30 min drug exposure (Fig. 4).

The emission spectra in cells treated with ST1481, obtained after subtraction of the natural fluorescence spectrum, exhibited a main emission band in the 450–520 nm region. Only small changes were found in the emission spectral shape between the two cell lines, and appeared to be independent from the incubation time (data not shown).

Similarly to TPT, the time course of the fluorescence emission signal in cells treated with ST1481 (10 μg/mL) showed a maximum after 30 min of drug exposure, followed by a decrease at longer times (Fig. 4). In contrast to TPT, the difference in ST1481 fluorescence signals between HT-29 and HT-29/Mit cells was marginal. This behavior was consistent with a comparable intracellular accumulation of ST1481 in the two cell lines [5]. Incubation of ST1481-treated cells in drug-free medium resulted in a slight increase in the fluorescence values for all times considered. Again, the higher fluorescence intensity in ST1481-treated cells than that found in TPT-treated cells supported an increased intracellular content of ST1481 in both cell lines [5].

The different time course of the fluorescence properties of TPT, in particular the spectral shape which suggests an interaction at sites with different physico-chemical characteristics, was consistent with a different drug intracellular localization in the HT-29 and HT-29/Mit cells. On the contrary, the much smaller changes in the fluorescence properties of ST1481, indicate no relevant differences in its intracellular localization sites.

3.3. Subcellular localization of the drugs

The subcellular localization sites of TPT and ST1481 were investigated by comparing their fluorescence patterns with those of cells stained with dyes specific for the cell organelles. Fluorescence patterns of cells stained with rhodamine 123, a mitochondrial stain, or with Lucifer Yellow, a marker of endosomal and endoplasmic compartment, or with LysoTracker Red, a lysosomal stain, are shown in Fig. 5. In both cell lines, TPT localized mainly in organelles quite resembling the mitochondrial structure (Fig. 5). The cationic and lipophilic features of TPT are consistent with its localization in mitochondria. The perinuclear accumulation and the occasional polar cytoplasmic diffusion of TPT can indicate a localization in the endoplasmic compartment. No coincidence was found between the localization pattern of TPT and that of LysoTracker Red. On the contrary, ST1481 intracellular localization was mostly superimposed to that of LysoTracker Red, in both HT-29 and HT-29/Mit cells, as verified on double stained samples (Fig. 6). However, the colocalization was not homogeneous, since some lysosomes did not take the drug and *vice versa*, suggesting that the intralysosomal localization is regulated by the environmental pH which is quite heterogeneous in these organelles.

In order to investigate the cellular basis of the different uptake and intracellular distribution of the two drugs in the

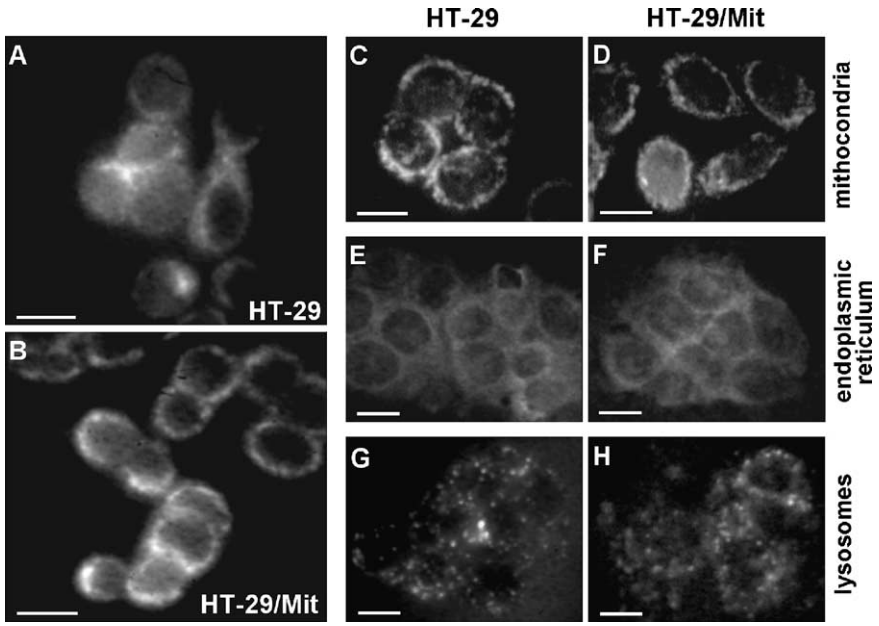

Fig. 5. Subcellular localization of TPT in HT-29 (A) and HT-29/Mit (B) cells after 1 hr of TPT exposure (10 μg/mL). The subcellular distribution of Rhodamine 123 (mithochondria—C, D), Lucifer Yellow (endoplasmic reticulum—E, F) and LysoTracker (lysosomes—G, H) in HT-29 (C, E, G) and HT-29/Mit cells (D, F, H) is shown for comparison. Excitation 366 nm, emission 440–520 nm (A, B, C–F); excitation 366 nm, emission >570 nm (G, H). Bars = 12 μm.

two cell lines, the expression and localization of BCRP, a protein implicated in TPT transport [10], has been examined. A different intracellular distribution of the protein in the two cell lines (Fig. 7) was evidenced by confocal microscopy. In HT29 cells, BCRP is found on cell membrane and inside the cytoplasm. In the resistant subline, BCRP is almost exclusively localized on the cell membrane.

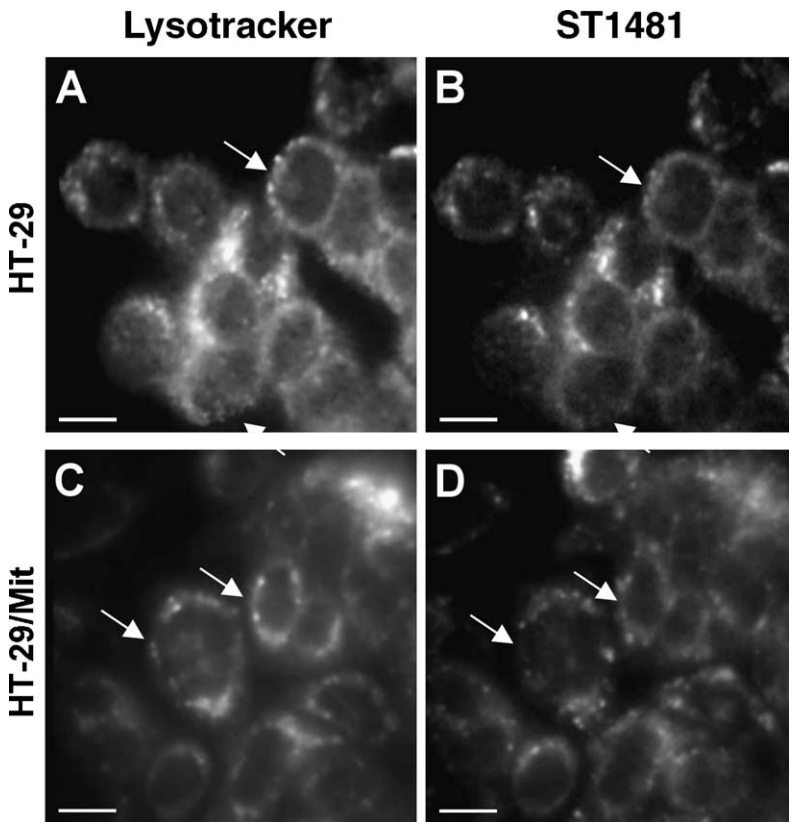

Fig. 6. Subcellular localization of ST1481 in HT-29 (A, B) and HT-29/Mit (C, D) cells after exposure to the drug (10 μg/mL, 1 hr) or LysoTracker Red. Panels A and C: LysoTracker (excitation 366 nm, emission 440–520 nm); panels B and D: ST1481 (excitation 366 nm, emission >570 nm). Bars = 12 μm. See Section 2 for details.

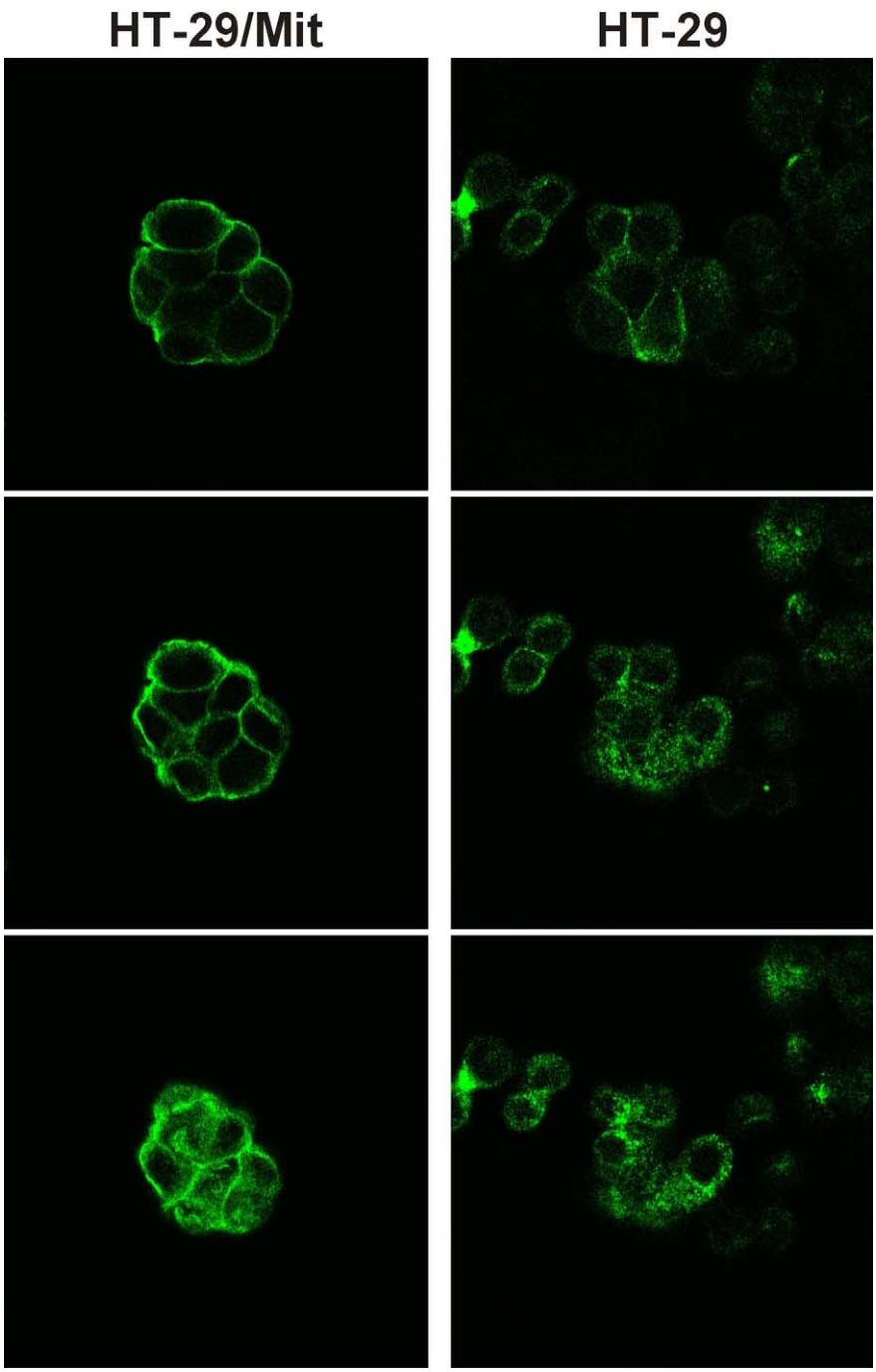

Fig. 7. Subcellular localization of BCRP. Pictures were taken by confocal microscopy. Three *z*-axis sections (HT-29 and HT-29/Mit) are reported for each observation.

3.4. Image analysis and fluorescence intensity in subcellular areas

The high-sensitivity image analysis showed a prevailing cytoplasmic localization of the fluorescence signal for both TPT and ST1481. For both cell lines the highest fluorescence emission signal of the two drugs occurred mostly in cytoplasmic granular structures. A detailed quantitative study of the intracellular localization of the two drugs was performed on single-cell images by means of a pixel-by-pixel evaluation of the fluorescence signal in selected areas of granular structures, non-granular cytoplasmic areas, or nuclei. As described in Section 3.3, granular structures correspond mainly to mitochondria and endoplasmic compartment for TPT, and to lysosomes for ST1481. The values of fluorescence intensity as function of time for the different subcellular localization are shown in Fig. 8. In each subcellular compartment, TPT fluorescence values were higher in HT-29 than in HT-29/Mit. At all the times considered, significant differences were found

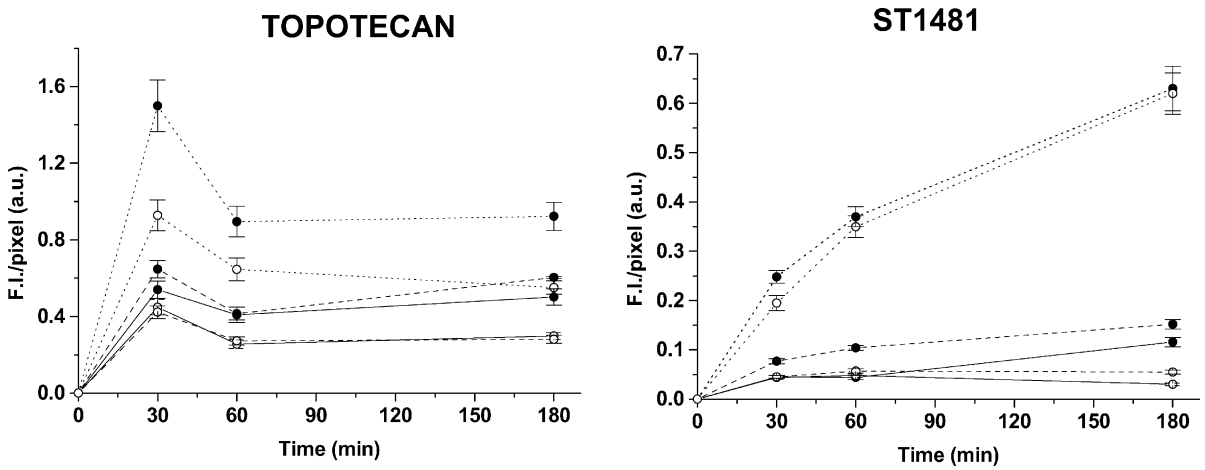

Fig. 8. Time course of fluorescence intensity in subcellular regions. Fluorescence intensities, expressed as F.I. mean values/pixel ± SE, were measured at $\lambda > 430$ nm in TPT and ST1481 treated HT-29 (●) and HT-29/Mit (○) cells by means of image analysis. Granules (. . .); cytoplasm (—); and nuclei (- - -).

for both the cytoplasmic granular areas and nuclei, that exhibited fluorescence signals about 60% lower in HT-29/Mit than in HT-29 cells. In non-granular cytoplasmic areas the difference between the two cell lines increased during time, and reached a maximum at 180 min. After 20-min incubation in drug-free medium, a slight decrease in the fluorescence emission was observed for all the subcellular areas considered in drug-loaded cells (not shown).

ST1481 fluorescence signals in granular structures were much higher, by about four times, than those recorded from the other cell areas, and were similar in HT-29 and HT-29/Mit cell lines. The greatest differences between the two cell lines were found for nuclei and cytoplasmic non-granular structures, by about three and four times respectively, at 180-min incubation time. In both cell lines, 20-min incubation in drug-free medium after drug uptakes resulted in a decrease in the granular fraction accompanied by an increase of the fluorescence emission in the diffuse cytoplasm (not shown). These results indicate a redistribution of the drug from the granules to the cytoplasm.

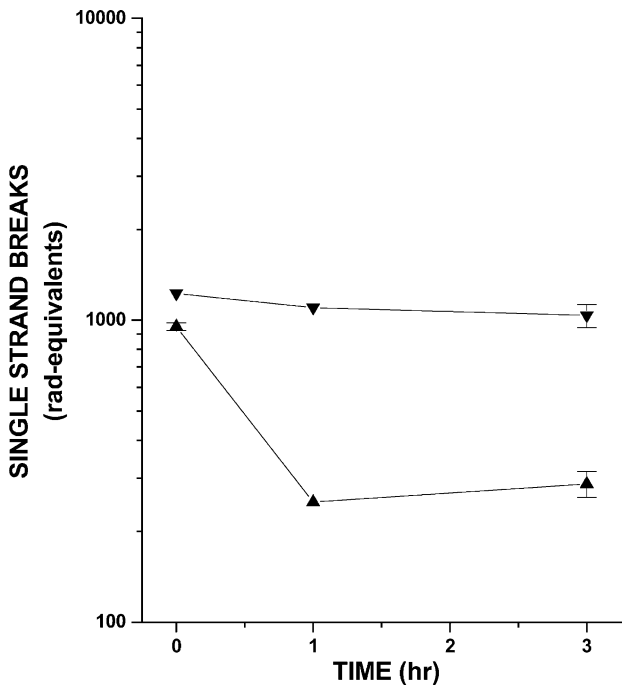

Fig. 9. Persistance of drug-induced DNA damage (single-strand breaks) in HT-29 cells. Following 1 hr exposure to the drug (IC_{80}, i.e. 10 and 0.55 μg/mL for topotecan and ST1481, respectively), cells were incubated in drug-free medium, for the indicated times. DNA single-strand breaks were determined by alkaline elution assay. TPT (▲) and ST1481 (▼).

3.5. Persistence of DNA damage

In spite of the well-known cytotoxic potency of camptothecins, the available evidence indicated that the major site of drug accumulation was not the nucleus. Since the primary target of these drugs is the nuclear enzyme DNA topoisomerase, we determined the extent and persistence of DNA damage in HT-29 cells following exposure to equitoxic concentrations of each drug (Fig. 9). Under these conditions, TPT was somewhat less effective than ST1481 in inducing single-strand DNA breaks. The most interesting finding of this study was a substantial persistence of DNA lesions in ST1481-treated cells, in contrast to a rapid damage recovery in TPT-treated cells. The formation of double-strand DNA breaks is a delayed event as a consequence of the processing of the topoisomerase I-DNA cleavable complex during DNA synthesis. As already observed in other cell lines [11], the extent of double-strand DNA breaks induced by the camptothecins was substantially lower and paralleled the extent of single-strand breaks (not shown).

4. Discussion

Microspectrofluorometric analysis of cells exposed to TPT evidenced a rapid initial increase in fluorescence signal, followed by a decrease, in agreement with data

already reported on a different cell line [12]. During incubation time differences were detected both in the spectral shape and in emission intensity between HT-29 and HT-29/Mit. The TPT fluorescence properties were found to be dependent on the polarity rather than on the pH of the medium. In particular, a blue-shift of the emission spectrum along with an increase in the fluorescence quantum efficiency was detected in the low polar medium dioxane, in agreement with already reported data [9]. The presence of the 10-hydroxyl group in the camptothecin fluorophore was reported to make TPT very sensitive to the microenvironment polarity [13], while neither the hydrolysis of the lactone, nor the protonization of the phenol group of the molecule were demonstrated to affect appreciably the emission shape, apart the appearance of a low contributing emission band at 425–435 nm at low pH values—protonated species—[14].

The changes in the position of TPT emission band during cells incubation indicate a relocalization of the drug in sites with various polarity degrees, which may be present to a different extent or are differently distributed in the two cell lines. In particular, the marked blue-shift of the emission band to 470 nm occurring in the HT-29/Mit cells in comparison with the parental cell line, indicates that the fraction of TPT that is not extruded by these cells, is retained in subcellular sites with low polarity properties. Since the spectral shift of TPT fluorescence is accompanied by a change in the quantum efficiency, a direct quantitative comparison of TPT levels cannot be performed among cells exhibiting different emission properties. An overestimation of the TPT level is to be expected in the case of 470 nm with respect to 525 nm emission band. For these reasons, our approach does not allow a comparison with data reported by Perego *et al.* [5] who showed a substantially increased accumulation of TPT in HT-29 with respect to HT-29/Mit cells at 60-min incubation. However, it is to be noted that at 30-min incubation, when both cell lines exhibit similar fluorescence properties, the fluorescence signal in HT-29 cells is about three times larger than in HT-29/Mit.

Microspectrofluorometric analysis of ST1481, as to spectral profile time course is concerned, showed that no appreciable changes occur in ST1481 fluorescence in the two cell lines, indicating that the drug localization sites in both HT-29 and HT-29/Mit cells have comparable chemico-physical properties. As to intracellular distribution, image analysis show less evident differences between the HT-29 and HT-29/Mit cell lines. It is to note that at 60 min of drug exposure, the HT-29/Mit cells exhibit greater fluorescence values than the parental line, in agreement with previous observations concerning cellular pharmacokinetics [5].

The different ability of HT-29 and HT29/Mit cell lines to handle TPT is consistent with a role of BCRP on the intracellular drug accumulation and relocalization. BCRP is expressed in both cell lines, but its cellular level is higher in HT-29/Mit than in HT29 cells, as already published by Perego *et al.* [5], and our results show that the BCRP localization is diffuse in the cytoplasm in HT-29 cells and almost exclusive in the plasmalemma of HT29/Mit cells. The intracellular distribution of TPT, that involves mainly mitochondria and endoplasmic reticulum, indicated a greater cytoplasmic diffuse pattern in HT-29 than in HT-29/Mit cells. In HT-29 cells, the marginal spectral shape changes support a prolonged persistence of the drug in the early localization sites. This can be related to the cytoplasmic presence of BCRP and to the consequent reduced ability of HT-29 to extrude TPT in comparison with HT-29/Mit cells. In these latter cells, the marked blue-shift, observed during time and the persistence of the 470 nm emission band after 60 min uptake, suggest both that BCRP is able to remove TPT rapidly from the early localization sites, and that TPT molecules, that are not extruded by BCRP, are sequestred in low polarity sites. All these results support the role of BCRP in recognizing TPT and determining its subcellular compartmentation and release from the cell.

In contrast to TPT, ST1481 showed fluorescence levels and intracellular localization very similar in the two cell lines at all the times considered. This finding is consistent with the previous observations indicating that ST1481 is not recognized by the BCRP transport system, thus its extrusion is not related to the cellular content or distribution of this protein.

A surprising observation of this study was the different subcellular localization of the two drugs, which are characterized by substantially different cytotoxic potency, being ST1481 at least 10 times more potent than TPT [5]. The increased intracellular accumulation of ST481, related to its lipophylic nature, could account for the cytotoxic potency. On the basis of the results presented in our study, the peculiar behavior of ST1481 at cellular level (i.e. localization in the lysosomal compartment) could contribute to the drug potency, because lysosomes represent a store allowing intracellular release of active drug (stabilized as lactone form in the acidic environment of the lysosomes).

The different subcellular localization of TPT and ST1481 is likely the result of different molecular interactions influenced by the different chemico-physical features related to the specific substituents at the 7 and 10 positions. In particular, the hydroxyl group at 10 position of TPT likely plays a relevant role in multiple molecular interactions including drug–protein interactions. Indeed, a water-soluble analogue related to ST1481 lacking the OH-group at position 10 exhibited a behavior comparable to ST1481 (not shown). Indeed, the spectral properties of TPT and ST1481 were markedly dependent on the environment, as evidenced by the spectrofluorometric analysis in solution under different polarity conditions.

In conclusion, the striking observation of a different subcellular localization of TPT and ST1481 supports that specific substituents in camptothecin molecule critically

influences the cellular pharmacology and likely the therapeutic properties. The present study further emphasizes the peculiar features of the novel camptothecin, gimatecan. In spite of the low water solubility, potential advantages of ST1481 could be: oral bioavailability, good pharmacological profile in terms of efficacy and tolerability, and favorable tissue distribution including ability to cross the blood–brain barrier.

Acknowledgments

The authors acknowledge the skillful assistance of Dr. Patrizia Vaghi, of the Centro Grandi Strumenti of the University of Pavia, Pavia, for the collection and processing of the fluorescence confocal images. This work was partially supported by the Associazione Italiana Ricerca sul Cancro, Milan, by the MIUR (FIRB Project), Rome, by the Ministero della Salute, Rome and by the T. Hoepli Foundation, Italy.

References

[1] Bailly C. Topoisomerase I poisons and suppressors as anticancer drugs. Curr Med Chem 2000;7:39–58.
[2] Zunino F, Dallavalle S, Laccabue D, Beretta G, Merlini L, Pratesi G. Current status and perspectives in the development of camptothecins. Curr Pharm Des 2002;8:2505–20.
[3] Dallavalle S, Delsoldato T, Ferrari A, Merlini L, Penco S, Carenini N, Perego P, De Cesare M, Pratesi G, Zunino F. Novel 7-substituted camptothecins with potent antitumor activity. J Med Chem 2000;43: 3963–9.
[4] De Cesare M, Pratesi G, Perego P, Carenini N, Tinelli S, Merlini L, Penco S, Pisano C, Bucci F, Vesci L, Pace S, Capocasa F, Carminati P, Zunino F. Potent antitumor activity and improved pharmacological profile of ST1481, a novel 7-substituted camptothecin. Cancer Res 2001;61:7189–95.
[5] Perego P, De Cesare M, De Isabella P, Carenini N, Beggiolin G, Pezzoni G, Palumbo M, Tartaglia L, Pratesi G, Pisano C, Carminati P, Scheffer GL, Zunino F. A novel 7-modified camptothecin analog overcomes breast cancer resistance protein-associated resistance in a mitoxantrone-selected colon carcinoma cell line. Cancer Res 2001; 61:6034–7.
[6] Allen JD, Schinkel AH. Multidrug resistance and pharmacological protection mediated by the breast cancer resistance protein (BCRP/ABCG2). Mol Cancer Ther 2002;1:427–34.
[7] Marquardt DW. An algorithm for least-squares estimation of nonlinear parameters. J Soc Ind Appl Math 1963;11:431–41.
[8] Kohn KW, Ewig RAG, Erickson LC, Zwelling LA. DNA repair. In: Friedberg EC, Hanawalt PC, editors. A laboratory manual of research procedures, vol. 1, part B. New York: Marcel Dekker; 1981. p. 370–401.
[9] Gryczynski I, Gryczynski Z, Lakowicz JR, Yang D, Burke TG. Fluorescence spectral properties of the anticancer drug topotecan by steady-state and frequency domain fluorometry with one-photon and multi-photon excitation. Photochem Photobiol 1999;69:421–8.
[10] Kruijtzer CMF, Beijnen JH, Rosing H, ten Bokkel Huinink WW, Schot M, Jewell RC, Paul EM, Schellens JHM. Increased oral bioavailability of topotecan in combination with the breast cancer resistance protein and P-glycoprotein inhibitor GF120918. J Clin Oncol 2002;20: 2943–50.
[11] Zuco V, Supino R, De Cesare M, Carenini N, Perego P, Gatti L, Pratesi G, Pisano C, Martinelli R, Bucci F, Zanier R, Carminati P, Zunino F. Cellular bases of the antitumor activity of a 7-substituted camptothecin in hormone-refractory human prostate carcinoma models. Biochem Pharmacol 2003;65:1281–94.
[12] Gabr A, Kuin A, Aalders M, El-Gawly H, Smets LA. Cellular pharmacokinetics and cytotoxicity of camptothecin and topotecan at normal and acidic pH. Cancer Res 1997;57:4811–6.
[13] Mi Z, Burke TG. Differential interactions of campothecin lactone and carboxylate forms with human blood components. Biochemistry 1994; 33:10325–36.
[14] Chourpa I, Millot JM, Sockalingum GD, Riou JF, Manfait M. Kinetics of lactone hydrolysis in antitumor drugs of camptothecin series as studied by fluorescence spectroscopy. Biochim Biophys Acta 1998; 1379:353–66.